DOI: 10.1002/cbic.200700434

A Molecular Dynamics Study of the ASC and NALP1 Pyrin Domains at Neutral and Low pH

Zrinka Gattin and Wilfred F. van Gunsteren*[a]

The pyrin domain is one of four subfamilies of the death domain superfamily of proteins, all members of which share a similar three-dimensional fold with a structure comprising five or six antiparallel α-helices. The pyrin domain of the ASC (six-helical fold) and of the NALP1 (five-helical fold) proteins were simulated at two different pH values, 3.7 and 6.5, with two different force-field parameter sets, and the molecular dynamics simulation trajectories were compared to NMR experimental data. The two force fields that were used did not show very different results. The simulations of NALP1 at pH 6.5 largely satisfied the experimental NOE atom–atom distance bounds that were measured at pH 6.5, and preserved its tertiary structure. The simulations at pH 3.7 showed a denaturation of the protein. The simulations of ASC at pH 3.7 only satisfied the experimental NOE atom–atom distance bounds that were measured at pH 3.7 if either three acidic side chains (Asp48, Glu64 and Asp75) or only two (Glu64 and Asp75) were not protonated. This indicates that the ASC tertiary structure is stabilized by salt bridges at low pH. A corresponding analysis for NALP1 at pH 3.7 only yielded one possible salt bridge, but this did not stabilize the tertiary structure at low pH. The results show that the particular protonation states of acidic side chains in the protein interior might be crucial to properly modeling these proteins at low pH.

Introduction

Until recently, the death domain superfamily of proteins was thought to consist of three subfamilies, the death domain (DD), the death effector domain (DED), and the caspase recruitment domain (CARD) proteins. In 1997 a fourth member of the death domain superfamily was found[1,2] and recognized based on sequence alignments, secondary structure predictions and homology modeling.[3–9] It was named the pyrin domain (PYD or PAAD, DAPIN, PLM, PYRN, PyK[3–6,8,9]) after the first protein in which it was discovered, pyrin (or marenostrin), a protein that regulates inflammatory signaling in myeloid cells.[10,11] Although no strong sequence similarity between the death domain subfamilies was found, they share a similar three-dimensional fold called the Greek key, which is an interaction domain that contains six antiparallel α-helices.

There are at least 19 genes that encode pyrin domain proteins in the human genome.[12] Mutations in the part of the genome that encodes the pyrin domain are connected with many hereditary diseases such as familial Mediterranean fever[1,2] (FMF), familial cold autoinflammatory syndrome (FCAS), chronic infantile neurological cutaneous and articular syndrome (CINCA), and Muckle–Wells syndrome (MWS); this points to the role of pyrin domain proteins in the control of inflammatory response.[13–18] Pyrin domains interact through specific homotypic protein–protein interactions (PPI)[4] that mediate interactions among proteins that are involved in the activation of inflammatory caspases (e.g., caspase-1) and NF-κB.[14,15,19–21] Although the nature of the interaction of pairs of pyrin domains is not yet resolved, experimental and molecular modeling studies suggest a role of charged and hydrophobic residues.[22,23]

Two proteins that have at their N terminus the pyrin domain and at their C terminus the CARD domain, the NALP1[24] (also called DEFCAP, CARD7 or NAC[3,25,26]) and ASC[22] (also called TMS1 or Pycard[4,27,28]) have raised our interest. NALP1 was the first NALP-family protein to be discovered by its sequence homology to APAF-1.[4,25,26] The role of the NALP1 protein in apoptotic pathways was suggested to be either via direct association with caspase-2 and caspase-9,[25] or indirectly through the interaction with APAF-1 and a subsequent enhancement of the apoptosome function,[26] or an activation of the proinflammatory caspases together with the ASC protein.[4,19] ASC was initially identified as a detergent-insoluble protein that forms filament-like structures (specks) in cells that are undergoing retinoic-acid-induced apoptosis.[29] ASC is abundantly expressed in many epithelial cells and leukocytes, hair follicles and peripheral blood lymphocytes.[30] The PYD of ASC interacts with the PYD of several NALP's, whereas ASC's CARD recruits the CARD of procaspase-1,[15,20,31] thereby producing an intracellular complex, the inflammasome. For more detailed reading on the topics of apoptosis, inflammation or the pyrin domain, we suggest the review articles of Reed et al.,[32] Mariathasan and Monack[33] and Kohl and Grütter.[9]

As previously mentioned, in the current study we consider the pyrin domains of two human proteins, NALP1[24] and ASC,[22] for which structures have been determined by NMR spectroscopy, albeit at different pH values (Figure 1). Although

[a] *Z. Gattin, Prof. Dr. W. F. van Gunsteren*
Laboratory for Physical Chemistry, ETH Zürich
Hoenggerberg, HCI G236, 8093 Zürich (Switzerland)
Fax: (+41) 44-632-1039
E-mail: wfvgn@igc.phys.chem.ethz.ch

 © 2008 Wiley-VCH Verlag GmbH & Co. KGaA, Weinheim

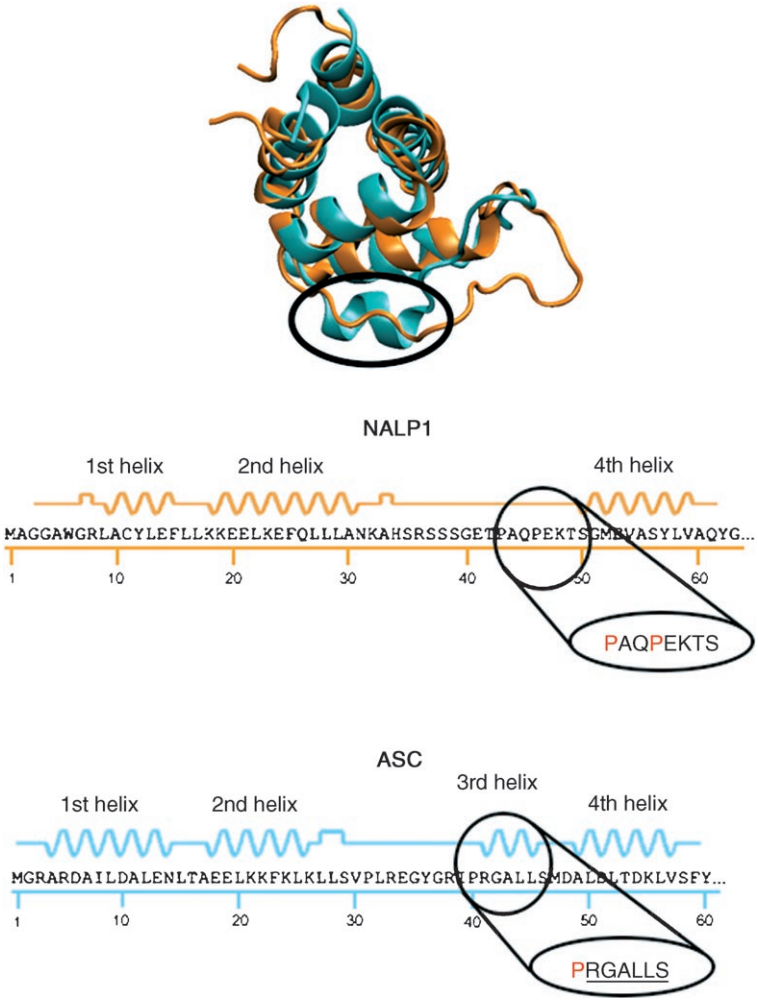

Figure 1. Structure (top) and sequence (bottom) comparison of the NMR structures[22,24] of part of the pyrin domains of the ASC (light blue) and NALP1 (orange) proteins. The third helix is circled in black.

both pyrin domains are members of the same pyrin domain subfamily, the ASC pyrin domain has six antiparallel helices, which fold is common to the pyrin domain subfamily, whereas the NALP1 pyrin domain lacks the third helix.

Until now only two additional structures of pyrin domains from human proteins have been determined by NMR spectroscopy analysis, and they contain the third helix.[34,35] The structure of the single domain protein, human ASC2 was determined by two different groups,[34,36] although they reported different structures. Espejo and Patarroyo[36] reported a five-helical structure that was based on NMR spectroscopy data that lacked the third helix, while the NMR spectroscopy analyses of Natarajan et al.[34] document the third helix, and differences in the orientation of helices 2 and 4.

Here we investigate whether molecular modeling and molecular dynamics (MD) simulations could provide us with the reason for the absence of the third helix in NALP1 PYD. Several MD simulations were performed with two GROMOS force fields, 45A4[37,38] and 53A6,[39,40] from which we analyze the possible effect of pH, amino acid sequence and force field. The performed simulations are summarized in Table 1.

The older GROMOS 45A4 force field does not yield sufficiently negative solvation free energies of polar moieties in water.[39] Therefore, the charge distributions and van der Waals parameters of such moieties were recalibrated against experimental hydration free energies, to give the 53A6 force field. The 53A6 parameter set describes the solvation free energies of polar and nonpolar moieties in various solvents very well.[41]

Table 1. Overview of the simulations that were performed. Two GROMOS force field parameter sets, 45A4 and 53A6, were used in the simulations.[a]

Simulation label	Force field parameter set	Box type	pH	Number of counterions	Protein total charge[e]
ASC_45A4_3.7	45A4	t	3.7	12	+12
ASC_53A6_3.7	53A6	t	3.7	12	+12
ASC_45A4_6.5	45A4	c	6.5	2	−2
ASC_53A6_6.5	53A6	c	6.5	2	−2
ASC_3sb_45A4_3.7	45A4	c	3.7 3sb	9	+9
ASC_3sb_53A6_3.7	53A6	c	3.7 3sb	9	+9
ASC_2sb_45A4_3.7	45A4	c	3.7 2sb	10	+10
NALP1_45A4_6.5	45A4	t	6.5	2	−2
NALP1_53A6_6.5	53A6	t	6.5	2	−2
NALP1_45A4_3.7	45A4	c	3.7	12	+12
NALP1_53A6_3.7	53A6	c	3.7	12	+12
NALP1_1sb_45A4_3.7	45A4	c	3.7 1sb	11	+11
NALP1_1sb_53A6_3.7	53A6	c	3.7 1sb	11	+11

[a] The pH values indicate different charge states for the ionizable (side chain, N and C terminal) moieties. The index "sb" indicates that the side chains of Glu52 in NALP1 ("1sb") or of Asp48, Glu62 and Asp75 in ASC ("3sb") or only of Glu62 and Asp75 in ASC ("2sb") are not protonated at low pH, which enables them to form salt bridges with Lys47 (NALP1) or (Lys24), Arg5, and Lys26 (ASC), respectively. All simulations are of 10 ns duration. Box type: cubic (c) or truncated octahedron (t); counterions: either Na^+ or Cl^-. The simulation label contains the following information: protein name, sb if nonstandard protonation state of particular side chains, force field parameter set, and pH value, all separated by underscores.

 © 2008 Wiley-VCH Verlag GmbH & Co. KGaA, Weinheim

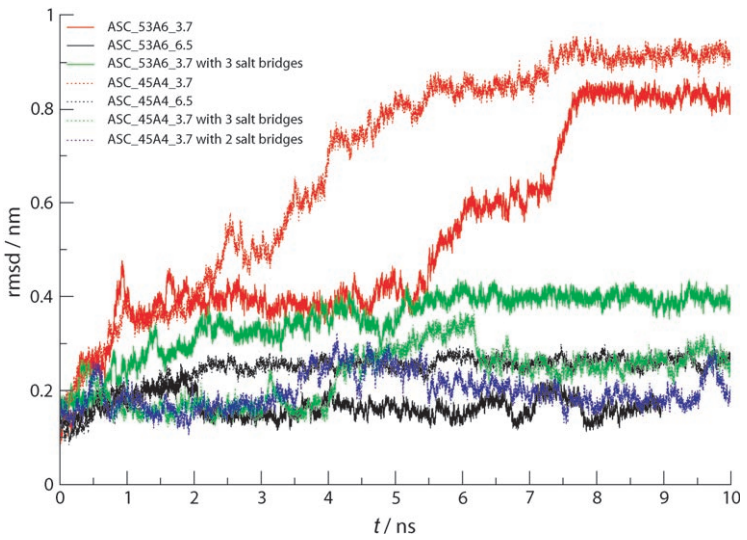

Figure 2. Backbone atom-positional root-mean-square difference (RMSD; excluding the third loop residues 27 to 40), of the trajectory structures with respect to the energy-minimized NMR structure as a function of time for the pyrin domain of the ASC protein (ASC PYD). Full lines correspond to the simulations with the GROMOS 53A6 force field, and dotted ones to the 45A4 one. Red lines are the simulations at pH 3.7, black lines at pH 6.5, green lines at pH 3.7 with Asp48, Glu64 and Asp75 deprotonated, and the blue line at pH 3.7 with Glu64 and Asp75 deprotonated.

In the sequence of the NALP1 pyrin domain in the region where we would expect the third helix to form (just before the fourth helix), a proline residue (at position 46) occurs, see Figure 1, which explains the absence of the third helix in NALP1. The simulations of NALP1 at pH 6.5, the pH for which the structure was experimentally determined,[24] show a stable fold. However, the simulations of ASC at pH 3.7, the pH for which the structure was experimentally determined,[22] show unfolding, see Figure 2. In the pH 3.7 simulations all Asp and Glu residues were protonated, which prevented them from forming strong salt bridges with Arg or Lys residues. The absence of salt-bridge interactions was considered to be a possible cause of the unfolding of ASC at pH 3.7.[42] Therefore, we investigated the role of salt bridges Lys47–Glu52 in NALP1, and Lys24–Asp48, Arg5–Glu62 and Lys26–Asp75 in ASC.

Results and Discussion

ASC PYD

We simulated the ASC pyrin domain at two pH values, at pH 3.7, at which its NMR spectroscopy structure was determined, and at pH 6.5, at which the NMR spectroscopy structure of the NALP1 pyrin domain was determined. At both pH values we used two GROMOS force fields: parameter sets 45A4 and 53A6 (Table 1).

The atom-positional root-mean-square deviations (RMSDs) of the simulation trajectory structures from the energy-minimized NMR spectroscopy structure (pH 3.7) for the backbone (N, C_α, C) atoms in the simulations ASC_45A4_3.7 and ASC_53A6_3.7, and in the simulations ASC_45A4_6.5 and ASC_53A6_6.5 are shown in Figure 2. The RMSD was calculated by excluding the third loop residues (27 to 40), which made it feasible to capture just the RMSD movement of the helices. For the two simulations at pH 3.7, the RMSD values increased within 10 ns of simulation time to a value of 0.9 nm and 0.8 nm when the force fields 45A4 and 53A6, respectively, were used. For the two simulations at pH 6.5, the behavior of the RMSD is quite the opposite; it reaches a plateau value of approximately 0.25 nm and 0.17 nm after 3 ns of simulation time for force fields 45A4 and 53A6, respectively. The increase in backbone RMSD to a value of about 0.9 nm for the simulations at pH 3.7 shows that the ensemble that is sampled by MD at pH 3.7 is structurally different from the NMR spectroscopy structure at pH 3.7, whereas the ensemble that is sampled by MD at pH 6.5 is close to the NMR spectroscopy structure at pH 3.7. This significant change in the simulated behavior of ASC PYD in going from pH 6.5 to pH 3.7, which is at odds with the NMR spectroscopy structure at pH 3.7, indicates that for the stabilization of the ASC structure at low pH, the chosen protonation states of Asp and Glu residues might not be appropriate. In other words, some electrostatic interactions, such as salt bridges or charge–dipole interactions, are likely to play a stabilizing role.

The atom-positional root-mean-square fluctuations (RMSFs) for the C_α atoms that were calculated for the whole 10 ns of the trajectories are shown in Figure 3, left panel for the simulations ASC_45A4_3.7 and ASC_45A4_6.5, and in Figure 3, right panel for the simulations ASC_53A6_3.7 and ASC_53A6_6.5. The two simulations at pH 3.7 show large fluctuations, not only in the loop region but also in the helical parts, in particular the third and fourth helices, whereas the two simulations at pH 6.5 show slightly enhanced fluctuations only in the loop region and at the chain termini. The big fluctuations at pH 3.7 are due to the unravelling of the fold.

In Figure 4, the secondary structure assignments as a function of time for the 45A4 simulation at pH 3.7 show that the helical structural elements are gradually lost, while they are preserved at pH 6.5 (data for the force field 53A6 are not shown).

A summary of the NOE atom–atom distance bound analysis can be found in Table 2. A total of 1117 NOE upper bounds (obtained at pH 3.7) were used in the analysis.[22] For the simulations at pH 3.7 the NOE analysis was done on an ensemble of structures that were taken from the last 2 ns of the simulation, because the backbone atom-positional RMSD from the starting structure is only stabilized after 8 ns (see Figure 2). For the simulations at pH 6.5 the NOE analysis was done on the ensemble of structures from the full 10 ns. The difference in the tertiary structure that was induced by the different pH states is strongly reflected in the NOE upper bound violations. At pH 3.7, a 10 to 30-fold increase of average NOE upper bound violations compared to pH 6.5 is found for both force fields (45A4 and 53A6).

 © 2008 Wiley-VCH Verlag GmbH & Co. KGaA, Weinheim

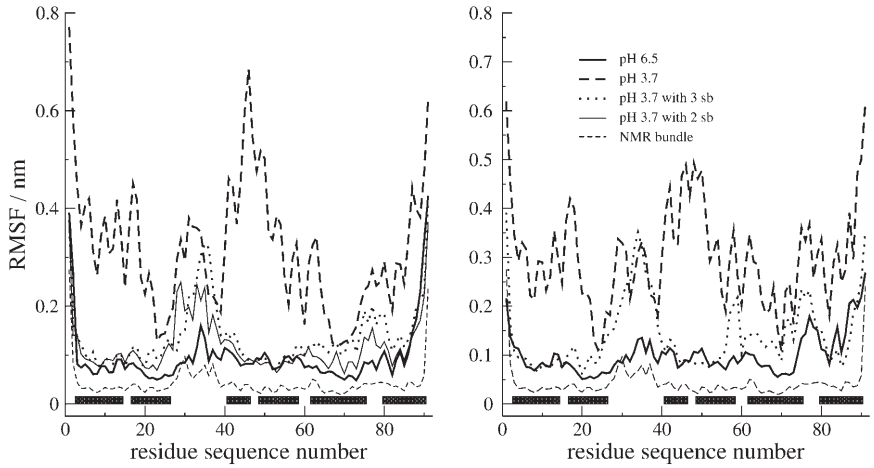

Figure 3. Atom-positional root-mean-square fluctuations (RMSF's) of the C_α atoms of ASC PYD in 10 ns simulations with force field 45A4 (left) and with 53A6 (right). Full thick black lines represent the simulations at pH 6.5, thick dashed lines that at pH 3.7, dotted lines those at pH 3.7 with Asp48, Glu64 and Asp75 deprotonated, the thin black line that at pH 3.7 with only Glu64 and Asp75 deprotonated, and the thin dashed lines represent the NMR bundle (20 structures). The positions of the 6 helices in the protein sequence are indicated with bars at the bottom of the graph.

NALP1 PYD

We also simulated the NALP1 PYD domain at two pH values, at pH 6.5, at which its NMR spectroscopy structure was determined, and at pH 3.7. At both pH values we used two GROMOS force fields: parameter sets 45A4 and 53A6 (Table 1).

The atom-positional RMSDs of the simulated trajectory structures from the NMR spectroscopy structure (pH 6.5) for the backbone (N, C_α, C) atoms, excluding the third loop residues (33 to 48), for the simulations NALP1_45A4_6.5 and NALP1_53A6_6.5, and the simulations NALP1_45A4_3.7 and NALP1_53A6_3.7 are shown in Figure 5. The RMSD values for the two simulations at pH 6.5 reach a plateau value of approximately 0.3 nm after 5 ns of simulation, but in the simulations at pH 3.7 they increase within 10 ns of simulation time to a value of about 1.0 nm for either force field. At pH 6.5, the ensemble that is sampled by MD is close to the NMR spectroscopy structure, whereas at pH 3.7 it is not. Because the NMR spectroscopy structure was determined at pH 6.5, this comes as no surprise.

The atom-positional RMSFs for the C_α atoms that were calculated for the whole 10 ns of the trajectories are shown in Figure 6, left panel, for the simulations NALP1_45A4_6.5 and NALP1_45A4_3.7, and in Figure 6, right panel, for the simulations NALP1_53A6_6.5 and NALP1_53A6_3.7. The two simulations at pH 6.5 show large fluctuations in the loop region and at the chain termini, but not in the helical parts, whereas the simulations at pH 3.7 show big fluctuations, particularly for the second and fourth helix.

The secondary structure assignments in Figure 7 show that at pH 6.5 the helical structural elements are preserved. For the simulations at pH 3.7 no substantial loss of secondary structure is observed as it was for the ASC simulation at pH 3.7.

A summary of the NOE atom–atom distance-bound analysis can be found in Table 2. A total of 1126 NOE upper bounds (obtained at pH 6.5) were used in the analysis.[24] For the simulations at pH 3.7, the NOE analysis was done on an ensemble of structures that were taken from the last 2 ns of the simulation. For the simulations at pH 6.5 the NOE analysis was done

Table 2. Number of NOE atom–atom distance upper bound violations and average violations in the simulations.[a]

Simulation label	pH	Averaging time period [ns]	Number of NOE upper bound violations $0.1 \le d < 0.2$ [nm]	$0.2 \le d < 0.3$ [nm]	$d \ge 0.3$ [nm]	Average violation [nm]
ASC_45A4_3.7	3.7	2	24	14	59	0.057
ASC_53A6_3.7	3.7	2	27	24	77	0.054
ASC_45A4_6.5	6.5	10	4	2	0	0.002
ASC_53A6_6.5	6.5	10	7	0	1	0.003
ASC_3sb_45A4_3.7	3.7	10 (2)	9 (7)	1 (5)	4 (10)	0.005 (0.009)
ASC_3sb_53A6_3.7	3.7	10 (2)	19 (29)	4 (19)	8 (46)	0.009 (0.032)
ASC_2sb_45A4_3.7	3.7	10 (2)	9 (17)	3 (6)	1 (4)	0.005 (0.007)
ASC_NMR	3.7	20 struct.	0	0	0	0.001
NALP1_45A4_6.5	6.5	10	19	6	8	0.009
NALP1_53A6_6.5	6.5	10	11	7	3	0.006
NALP1_45A4_3.7	3.7	2	39	32	124	0.122
NALP1_53A6_3.7	3.7	2	42	28	141	0.114
NALP1_1sb_45A4_3.7	3.7	10 (2)	30 (39)	24 (17)	12 (102)	0.017 (0.209)
NALP1_1sb_53A6_3.7	3.7	10 (2)	18 (32)	13 (16)	29 (78)	0.021 (0.102)
NALP1_NMR	6.5	20 struct	0	0	0	0.001

[a] For the simulations of ASC PYD a total number of 1117 NOE's that were obtained at pH 3.7,[22] and for the simulations of the NALP1 PYD a total number of 1126 NOEs that were obtained at pH 6.5[24] were considered. The simulation labels are defined in Table 1. The index "NMR" indicates the NMR bundle of 20 structures for the ASC and NALP1 proteins.

 © 2008 Wiley-VCH Verlag GmbH & Co. KGaA, Weinheim

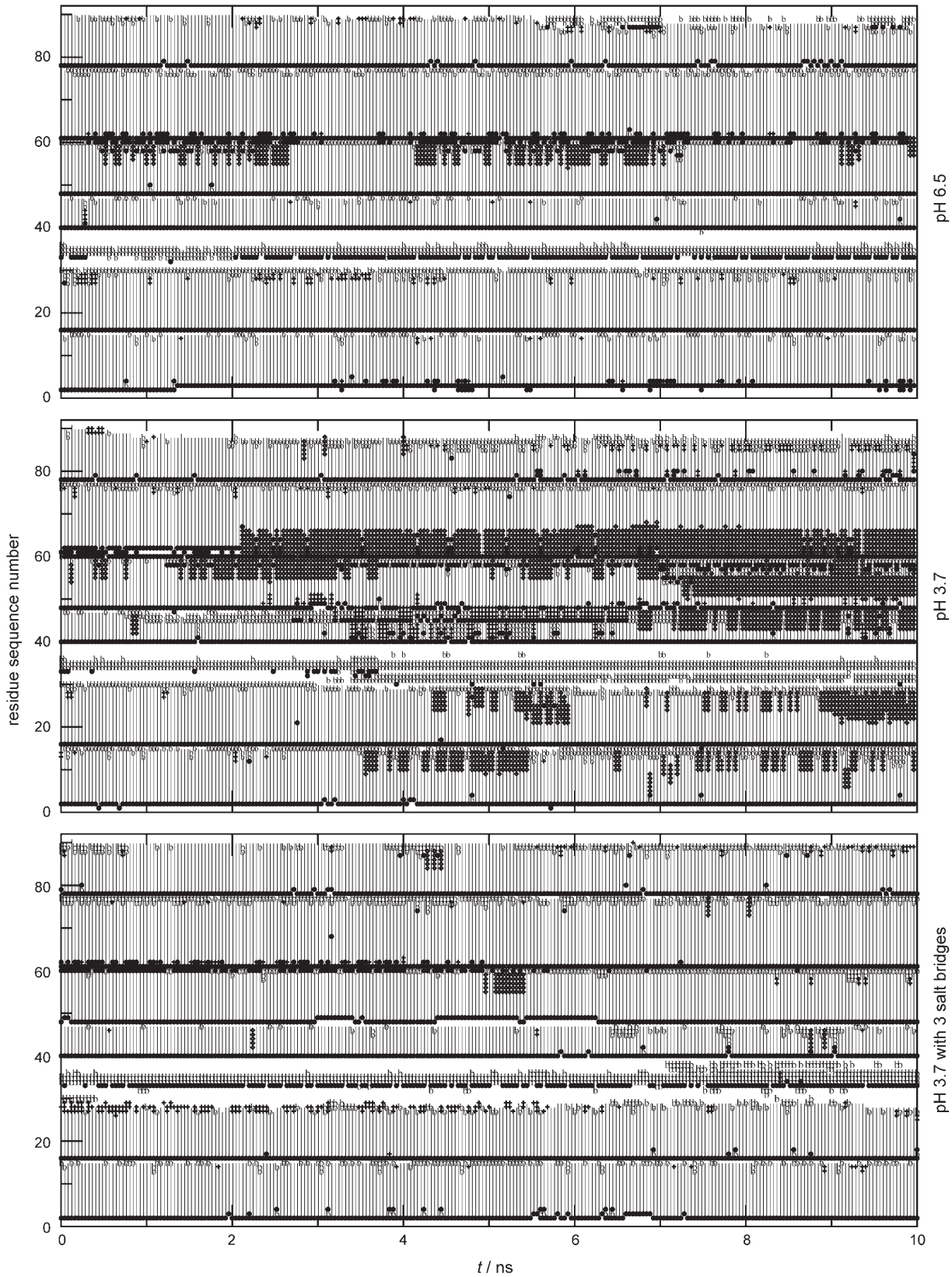

Figure 4. The secondary structure assignment (DSSP) of the ASC pyrin domain was calculated according to ref. [68], and was simulated with force field 45A4 at pH 6.5 (top), at pH 3.7 (middle) and at pH 3.7 with Asp48, Glu64 and Asp75 deprotonated (bottom). +: a 3-helix, |: a 4-helix, ◆: a 5-helix, "b": a bend, and a ●: a turn.

 © 2008 Wiley-VCH Verlag GmbH & Co. KGaA, Weinheim

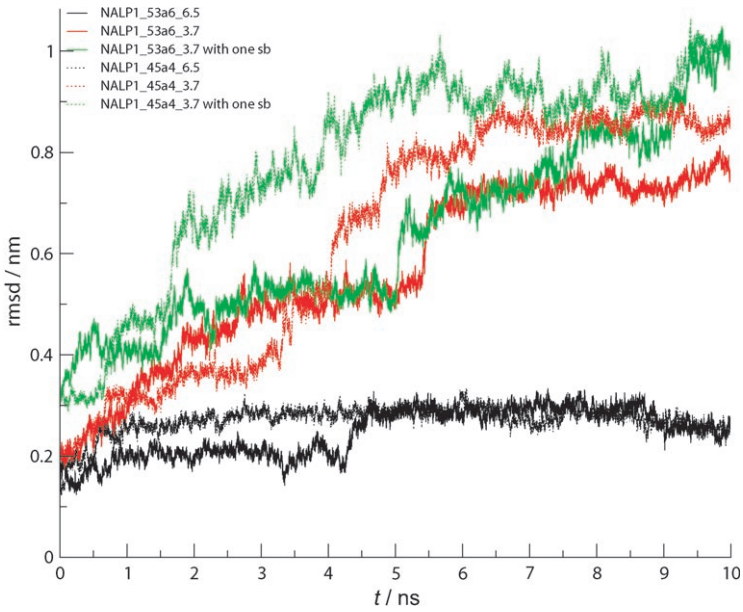

Figure 5. Backbone atom-positional RMSD (excluding the third loop residues 33 to 48), of the trajectory structures with respect to the energy-minimized NMR structure as a function of time for the pyrin domain of the NALP1 protein (NALP1 PYD). Full lines correspond to the simulations with the GROMOS 53A6 force field, and dotted ones to the 45A4 one. Red lines are the simulations at pH 3.7, black lines at pH 6.5 and green lines at a pH of 3.7 with Glu52 deprotonated.

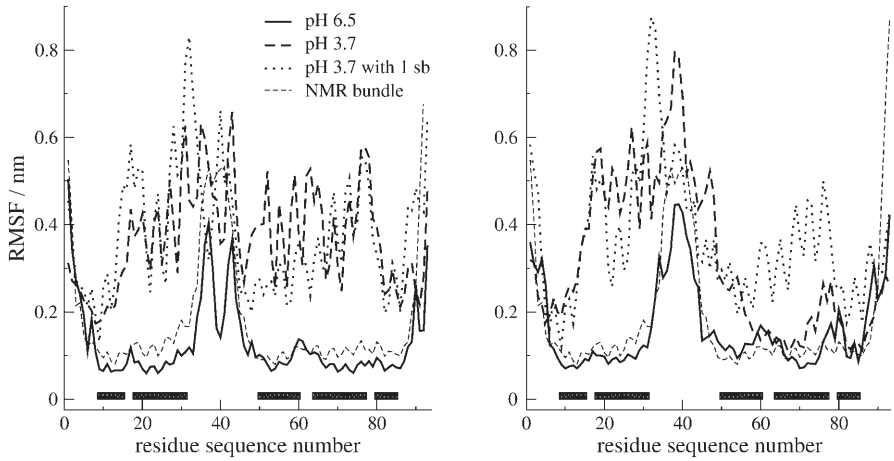

Figure 6. Atom-positional root-mean-square fluctuations (RMSF's) of the C_α atoms of NALP1 PYD in 10 ns simulations with force field 45A4 (left) and with 53A6 (right). Full thick black lines represent the simulations at pH 6.5, thick dashed lines represent those at pH 3.7, dotted lines represent those at pH 3.7 with Glu52 deprotonated, and the thin dashed lines represent the NMR bundle (20 structures). The positions of the 5 helices in the protein sequence are indicated with bars at the bottom of the graph.

on the ensemble of structures from the full 10 ns. The difference in the tertiary structure that was induced by the different pH states is strongly reflected in the NOE upper bound violations. At pH 3.7, a 10 to 20-fold increase of the average NOE upper bound violations compared to pH 6.5 is found for both force fields (45A4 and 53A6).

Salt bridges at low pH

As previously mentioned, the structure of ASC PYD as experimentally determined at pH 3.7 was not reproduced when simulated at pH 3.7, but it was when the simulations were performed at pH 6.5. The only differences between these two simulations were the protonation states of the 14 acidic amino acids (Asp and Glu) and the corresponding number of counterions. From the literature it is known that electrostatic interactions in salt bridges can play a stabilizing role. With this in mind, we searched for distances between the carboxyl C atoms in Asp and Glu side chains and the amine N atoms in Lys side chains, or amide N atoms in Arg side chains that are shorter than 1 nm. In this search, three distances between basic and acidic side chains were found (Figure 8) for ASC PYD, R5-E62, K24-D48 and K26-D75.

To test whether these contacts might play a stabilizing role, we performed simulations at pH 3.7 in which we left Asp48, Glu62 and Asp75 unprotonated while all other acidic amino acids were protonated (see Table 1). Figure 8 shows that all three contacts are conserved in the simulation at pH 3.7 with the deprotonated Asp48, Glu52 and Asp75 side chains.

The atom-positional RMSDs of the trajectory structures from the energy-minimized NMR spectroscopy structure (pH 3.7) for the N, C_α, C backbone atoms, excluding the third loop residues for the simulations ASC_3sb_45A4_3.7 and ASC_3sb_53A6_3.7 are shown in Figure 2. The RMSD values for the simulations with force field 45A4 and 53A6 at pH 3.7 reach a plateau value of approximately 0.3 nm and 0.4 nm, respectively, after 6 ns of simulation time, in contrast to the simulations at pH 3.7, which lack the three side-chain contacts.

The atom-positional RMSFs for the C_α atoms that were calculated for the whole 10 ns of the trajectories are shown in Figure 3, left panel, for the simulations ASC_3sb_45A4_3.7 (dotted line) and ASC_3sb_53A6_3.7 in Figure 3, right panel. In contrast to the RMSFs of the simulations at pH 3.7 without the side-chain contacts (dashed lines), the two simulations show only large fluctuations in the loop region. The secondary structure assignments (Figure 4) show that the helical structural elements are preserved during both simulations.

Also, the NOE analysis in Table 2 shows that the simulated ensemble now largely satisfies the NOE upper bounds. The

 © 2008 Wiley-VCH Verlag GmbH & Co. KGaA, Weinheim

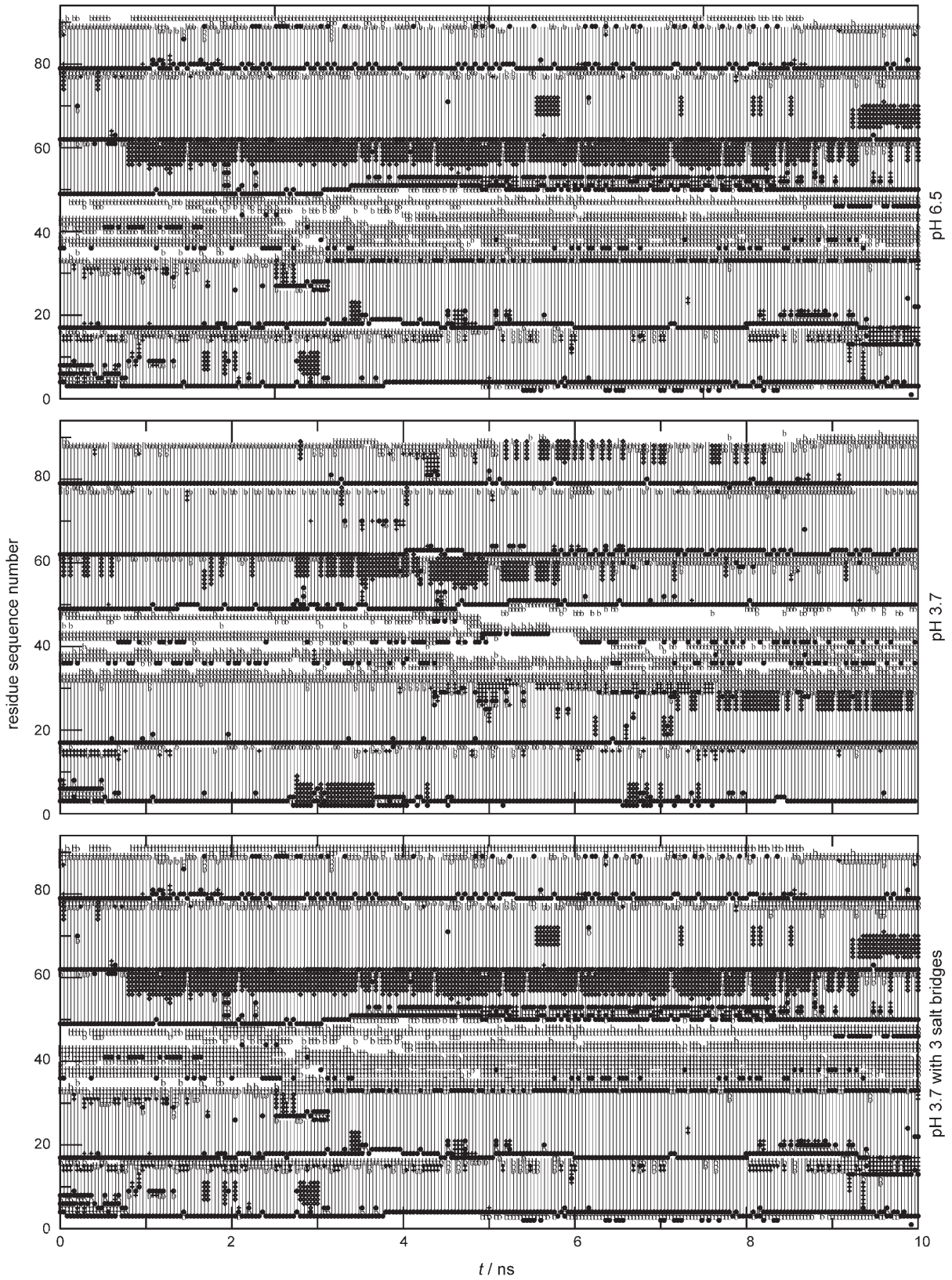

Figure 7. Secondary structure assignment (DSSP) of the NALP1 PYD that was simulated with force field 45A4 at pH 6.5 (top), at pH 3.7 (middle) and at pH 3.7 with Glu52 deprotonated (bottom). +: a 3-helix, |: a 4-helix, ◆: a 5-helix, "b": a bend, and a ●: a turn.

 © 2008 Wiley-VCH Verlag GmbH & Co. KGaA, Weinheim

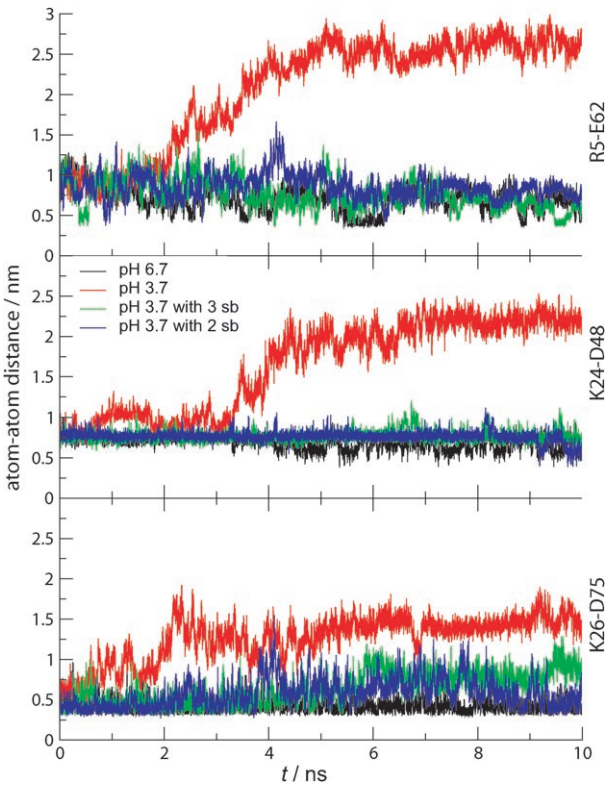

Figure 8. Atom–atom distances of three salt-bridge contacts as a function of time for ASC PYD for the simulations with force field 45A4. Upper panel: distance between the amide N atom of Arg5 and the carbonyl C atom of Glu62. Middle panel: distance between the amine N atom of Lys24 and the carbonyl C atom of Asp48. Bottom panel: distance between the amine N atom of Lys26 and the carbonyl C atom of Asp75. Black lines represent the simulations at pH 6.5, red lines the simulations at pH 3.7, green lines the simulations at pH 3.7 with Asp48, Glu64 and Asp75 deprotonated, and blue lines the simulations at pH 3.7 with only Glu64 and Asp75 deprotonated.

three side-chain contacts clearly stabilize the ASC structure at pH 3.7.

To verify that these contacts represent salt bridges, an analysis of the side-chain configurations was performed (local orientation of the charged part of the residues, results not shown) for the simulations at pH 6.5 and at pH 3.7 with the deprotonated Asp48, Glu52 and Asp75 side chains. It was found that the orientation of Asp48 changed such that it did not make a salt-bridge contact. Instead, Asp48 made a charged hydrogen bond interaction with protonated Asp51, whereas Lys24 made a tightly charged interaction with the backbone C=O of residue 47. The other two side-chain contacts that involve the deprotonated Glu52 and Asp75 side chains appeared to stay in salt-bridge form through the full simulation time. To test whether these two out of the three salt-bridge contacts are sufficient to stabilize the tertiary structure, a simulation with only deprotonated Glu52 and Asp75 side chains was performed.

The atom-positional RMSDs of the trajectory structures from the energy-minimized NMR spectroscopy structure (pH 3.7) for the N, C_α, C backbone atoms, excluding the third loop residues for the simulation ASC_2sb_45A4_3.7, are shown in Figure 2. Through the 10 ns simulation time there was no indication from the RMSD analysis that the ASC protein in the ASC_2sb_45A4_3.7 simulation was less stable than ASC in the simulation with deprotonated Asp48, Glu52 and Asp75 side chains. The RMSD value for the simulation with the 45A4 force field reached a plateau value of approximately 0.2 nm.

The atom-positional RMSFs for the C_α atoms that were calculated for the whole 10 ns of the trajectories are shown in Figure 3, left panel, for the simulation ASC_2sb_45A4_3.7 (thin line). There are no significant differences in the RMSF of the ASC_3sb_45A4_3.7 and ASC_2sb_45A4_3.7 simulations. The secondary structure assignments (not shown) show that the helical structural elements are preserved during the simulation.

Also the NOE analysis in Table 2 shows that the simulated ensemble for the ASC_2sb_45A4_3.7 simulation satisfies the NOE upper bounds. The two salt bridges play an essential role in stabilizing the ASC structure at pH 3.7.

A similar salt bridge distance analysis was performed for the NALP1 protein. In this case only one salt-bridge contact in the protein was found, Lys47–Glu52. Simulations at pH 3.7 with Glu52 deprotonated were performed and analyzed as before: the atom-positional RMSD from the NMR spectroscopy structure is shown in Figure 5, the atom-positional RMSF values are in Figure 6, the secondary structure analysis is in Figure 7, and the Lys47–Glu52 salt-bridge distance is in Figure 9. These data show that this single salt bridge is not able to stabilize the NALP1 structure at low pH.

The results that were obtained show that the particular protonation states of acidic side chains might be of crucial importance to the stability of the tertiary fold of the protein at low pH. At this point one could think of calculating the pK_A value of the mentioned Asp and Glu side chains by solving the Poisson–Bolzmann (PB) equation,[43] thus modeling a continuum solvent around the protein. A variety of difficulties are encountered when calculating pK_A values by solving the PB equation. On the one hand, there are several parameters for which a value has to be chosen, or that can be determined by fitting to a given set of pK_A values: the partial atomic charges and van der Waals radii of atoms[44,45] and values for the dielectric constant inside and outside the protein.[46–49] On the other hand, the accuracy of a continuum solvent model can be questioned, especially for protonation sites close to the continuum solvent. There the choice of the computational grid comes into play: whether a grid point lies just within the protein or just outside the protein can affect the calculated pK_A values significantly. Efforts have been made to alleviate this problem by introducing single explicit water molecules.[50,51] In addition, calculations that are based on a single structure of the protein neglect structural fluctuations and seem to be less accurate than calculations that are based on ensembles.[52] Alternative methods to compute pK_A values are based on microscopic polarization models[53,54] or the analysis of Gaussian fluctuations.[55] A review that compares different methods for calculating pK_A values of proteins can be found in ref. [56]. For these reasons we did not calculate pK_A values.

 © 2008 Wiley-VCH Verlag GmbH & Co. KGaA, Weinheim

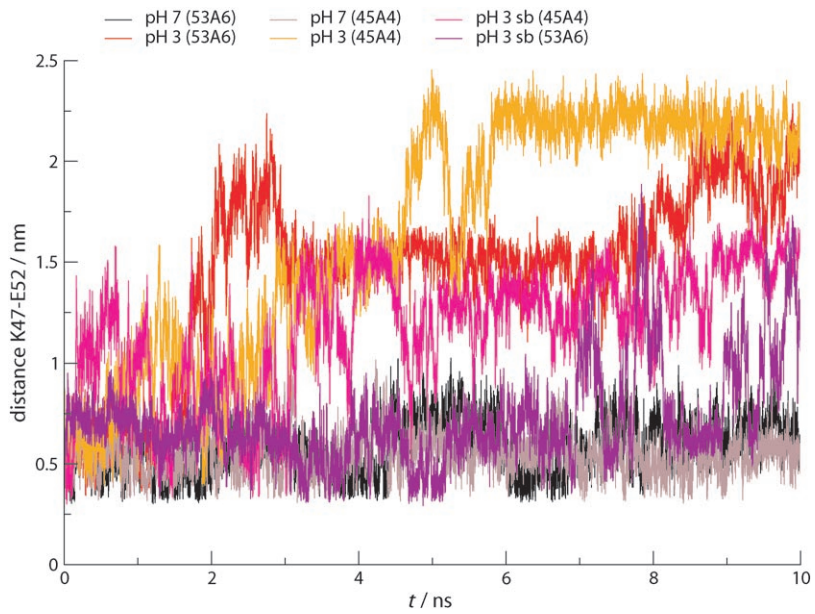

Figure 9. Atom–atom distance of one salt-bridge contact, between the amine N atom of the Lys47 side chain and the carbonyl C atom of the Glu52 side chain, as a function of time for NALP1 PYD. Black, red and violet lines represent the simulations with force field 53A6, whereas brown, orange and magenta lines represent the simulations with force field 45A4. Black and brown represent the simulation at pH 6.5, red and orange at pH 3.7, and violet and magenta at pH 3.7 with Glu52 deprotonated.

Experimental Section

Computational methods: The simulations (Table 1) were carried out in explicit solvent by using the GROMOS96 biomolecular software[57,58] and force field parameter sets 45A4[37,38] and 53A6.[39,40] The initial coordinates were taken from the NMR structure of NALP1 (PDB entry: 1pn5[24]) and of ASC (PDB entry: 1ucp[22]). The simple-point-charge (SPC) water model[59] was used to describe the solvent molecules. Aliphatic CH_n groups were treated as united atoms.[60]

The different pH values were mimicked by different protonation states of acidic residues.[61] For all simulations at both pH values the N termini were protonated, and the C termini were deprotonated. All acidic residues were protonated (Asp, Glu) at pH 3.7 (zero charge), only in the simulations with salt bridges ("sb") were specific acidic residues left deprotonated. His residues were deprotonated at pH 6.5, and protonated at pH 3.7, whereas Arg and Lys were protonated at all pH values. The total charge of a given protein and the corresponding numbers of counterions to neutralize the system are shown in Table 1.

Simulation setup: Periodic boundary conditions were applied based on a truncated octahedron or a cubic box (see Table 1). The protein in each simulation was solvated in water by enforcing a minimum distance of 1.2 nm or 1.4 nm between any atom and the nearest box wall for a truncated octahedron or a cubic box, respectively. In all simulations counterions were present in different quantities (shown in Table 1), such that the overall charge of the system was zero. Counterions were placed randomly in the simulation box with a minimal distance between the protein atoms and the ions of 0.35 nm. Steepest-descent energy minimization was performed, in which the protein atoms were positionally restrained by using a harmonic interaction with a force constant of 2.5×10^4 kJ mol^{-1} nm^{-2}. A succeeding steepest-descent energy minimization of the system was performed with the goal of relaxing the solvent–solute contacts, while positionally restraining only the backbone atoms of the solute by using a harmonic interaction with a force constant of 2.5×10^4 kJ mol^{-1} nm^{-2}. Bond lengths were constrained by application of the SHAKE algorithm[62] with a relative geometric tolerance of 10^{-4}. Long-range interactions were handled by using a triple-range cut-off scheme[63,64] with cut-off radii of 0.8 nm and 1.4 nm. Short-range van der Waals and electrostatic interactions were evaluated at every time step based on a charge-group pair list. Medium-range interactions, between 0.8 and 1.4 nm cut-off radii, were evaluated at every fifth step, at which time the pair list was updated. Outside the longer cut-off radius of 1.4 nm, a reaction-field approximation[64] was used with a relative dielectric permittivity of 61.[65]

The initial velocities of the atoms were assigned from a Maxwell distribution at 100 K, followed by a 2.5 ps period of MD simulation with harmonic position restraining of the solute atoms with force constants of 2.5×10^4 kJ mol^{-1} nm^{-2}. Succeeding equilibrations of 50 ps each, with force constants of 2.5×10^2, 2.5×10^1, 2.5×10^0 kJ mol^{-1} nm^{-2} and no restraining were performed on the systems at 150, 200, 250 and 298 K, respectively.

After an initial equilibration period of 200 ps, the simulations were continued for 10 ns and the analysis was based on configurations that were saved every 0.5 ps. The simulations were performed at 298 K (the experimental temperature of the ASC system was 301 K, whereas for NALP1 it was 293 K). Solute and solvent temperatures were maintained independently by weak coupling to two temperature baths of 298 K with relaxation times of 0.1 ps.[66] The pressure was calculated by using a molecular virial, and maintained by weak coupling to a pressure bath (isotropic coordinate scaling)[66] with a relaxation time of 0.5 ps by using an isothermal compressibility of 4.575×10^{-4} (kJ mol^{-1} nm^{-2})$^{-1}$. The equations of motion were integrated by using the leap-frog algorithm by using a timestep of 2 fs.

Analysis: Analyses were performed with the software GROMOS++.[67]

The atom-positional root-mean-square deviations (RMSD) from the reference structures were evaluated based on all backbone atoms (N, C_α, C) of all residues, except for the loop part of the molecule (residues 27 to 40 for ASC and residues 33 to 48 for NALP1). The superposition of structures was performed by using the same set of atoms. The reference structures were energy-minimized PDB structures. Atom-positional root-mean-square fluctuations (RMSF) over a period of simulation were calculated after superposition of centers of mass and performing a rotational atom-positional least-squares fit of the trajectory structures on the reference structure (energy-minimized PDB structures). The secondary structure assign-

 © 2008 Wiley-VCH Verlag GmbH & Co. KGaA, Weinheim

ment was done by using the program DSSP, based on the Kabsch–Sander rules.[68]

Comparisons to NMR experimental data were made through an analysis of proton–proton distances compared to nuclear Overhauser effect (NOE) upper bounds. For ASC PYD at pH 3.7,[22] 1117 NOE upper bounds were available, and for NALP1 PYD at pH 6.5,[24] 1126 NOE upper bounds were available. Proton–proton distances at 298 K were averaged by using $1/r^6$ averaging, that is, $r = (\{r^{-6}\})^{-1/6}$.

Acknowledgements

We thank Dr. Bojan Zagrovic for fruitful discussions and Prof. Dr. Markus Grütter for suggesting a computer simulation study of the stability of pyrin domain proteins. Prof. Dr. Kurt Wüthrich and Prof. Dr Gottfried Otting kindly provided the NOE data for NALP1 and ASC, respectively, which is gratefully acknowledged. Financial support was obtained from the National Center of Competence in Research (NCCR) Structural Biology of the Swiss National Science Foundation, which is gratefully acknowledged.

Keywords: death domain superfamily · molecular modeling · protein structures · pyrin domain · salt bridge

[1] The International FMF Consortium, *Cell* **1997**, *90*, 797–807.
[2] The French FMF Consortium, *Nat. Genet.* **1997**, *17*, 25–31.
[3] J. Bertin, P. S. DiStefano, *Cell Death Differ.* **2000**, *7*, 1273–1274.
[4] F. Martinon, K. Hofmann, J. Tschopp, *Curr. Biol.* **2001**, *10*, R118–R120.
[5] E. Staub, E. Dahl, A. Rosenthal, *Trends Biochem. Sci.* **2001**, *26*, 83–85.
[6] K. Pawlowski, F. Pio, Zhi-Liang Chu, J. C. Reed, A. Godzik, *Trends Biochem. Sci.* **2001**, *26*, 85–87.
[7] W. J. Fairbrother, N. C. Gordon, E. W. Humke, K. M. O'Rourke, M. A. Starovasnik, J.-P. Yin, V. M. Dixit, *Protein Sci.* **2001**, *10*, 1911–1918.
[8] D. Gumucio, A. Diaz, P. Schaner, N. Richards, C. Babcock, M. Schaller, T. Cesena, *Clin. Exp. Rheumatol.* **2002**, *20*, 45–53.
[9] A. Kohl, M. G. Grütter, *C. R. Biol.* **2004**, *327*, 1077–1086.
[10] M. Centola, G. Wood, D. M. Frucht, J. Galon, M. Aringer, C. Farrell, D. W. Kingma, M. E. Horowitz, E. Mansfield, S. M. Holland, J. J. O'Shea, H. F. Rosenberg, H. L. Malech, D. L. Kastner, *Blood* **2000**, *95*, 3223–3231.
[11] N. Richards, P. Schaner, A. Diaz, J. Stuckey, E. Shelden, A. Wadhwa, D. L. Gumucio, *J. Biol. Chem.* **2001**, *276*, 39320–39329.
[12] J. C. Reed, K. S. Doctor, A. Rojas, J. M. Zapata, C. Stehlik, L. Fiorentino, J. Damiano, W. Roth, S.-I. Matsuzawa, R. Newman, S. Takayama, H. Marusawa, F. Xu, G. Salvesen, RIKEN GER Group, GSL Members, A. Godzik, *Genome Res.* **2003**, *13*, 1376–1388.
[13] H. M. Hoffman, J. L. Mueller, D. H. Broide, A. A. Wanderer, R. D. Kolodner, *Nat. Genet.* **2001**, *29*, 301–305.
[14] G. A. Manji, L. Wang, B. J. Geddes, M. Brown, S. Merriam, A. Al-Garawi, S. Mak, J. M. Lora, M. Briskin, M. Jurman, J. Cao, P. S. DiStefano, J. Bertin, *J. Biol. Chem.* **2002**, *277*, 11570–11575.
[15] L. Wang, Gulam A. Manji, Jill M. Grenier, A. Al-Garawi, S. Merriam, J. M. Lora, B. J. Geddes, M. Briskin, P. S. DiStefano, J. Bertin, *J. Biol. Chem.* **2002**, *277*, 29874–29880.
[16] W. O'Connor, Jr., J. A. Harton, X. Zhu, M. W. Linhoff, J. P.-Y. Ting, *J. Immunol.* **2003**, *171*, 6329–6333.
[17] L. Agostini, F. Martinon, K. Burns, M. F McDermontt, P. N. Hawkins, *Immunity* **2004**, *20*, 319–325.
[18] C. Stehlik, J. C. Reed, *J. Exp. Med.* **2004**, *200*, 551–558.
[19] J. Tschopp, F. Martinon, K. Burns, *Nat. Rev. Mol. Cell Biol.* **2003**, *4*, 95–104.
[20] S. M. Srinivasula, J.-L. Poyet, M. Razmara, P. Datta, Z. Zhang, E. S. Alnemri, *J. Biol. Chem.* **2002**, *277*, 21119–21122.
[21] L. Fiorentino, C. Stehlik, V. Oliveira, M. E. Ariza, A. Godzik, J. C. Reed, *J. Biol. Chem.* **2002**, *277*, 35333–35340.
[22] E. Liepinsh, R. Barbals, E. Dahl, A. Sharipo, E. Staub, G. Otting, *J. Mol. Biol.* **2003**, *332*, 1155–1163.
[23] M. Moriya, S. Taniguchi, P. Wu, E. Liepinsh, G. Otting, J. Sagara, *Biochemistry* **2005**, *44*, 575–583.
[24] S. Hiller, A. Kohl, F. Fiorito, T. Herrmann, G. Wider, J. Tschopp, M. G. Grütter, K. Wüthrich, *Structure* **2003**, *11*, 1199–1205.
[25] T. Hlaing, R. F. Guo, K. A. Dilley, J. M. Loussia, T. A. Morrish, M. M. Shi, C. Vincenz, P. A. Ward, *J. Biol. Chem.* **2001**, *276*, 9230–9238.
[26] Z.-L. Chu, F. Pio, Z. Xie, K. Welsh, M. Karajewska, S. Karajewski, A. Godzik, J. C. Reed, *J. Biol. Chem.* **2001**, *276*, 9239–9245.
[27] K. E. Conway, B. B. McConnell, C. E. Bowring, C. D. Donald, S. T. Warren, P. M. Vertino, *Cancer Res.* **2000**, *60*, 6236–6242.
[28] B. B. McConnell, P. M. Vertino, *Cancer Res.* **2000**, *60*, 6243–6247.
[29] J. Masumoto, S. Taniguchi, K. Ayukawa, H. Sarvotham, T. Kishino, N. Niikawa, E. Hidaka, T. Katsuyama, T. Higushi, J. Sagara, *J. Biol. Chem.* **1999**, *274*, 33835–33838.
[30] J. Masumoto, *J. Histochem. Cytochem.* **2001**, *49*, 1269–1275.
[31] F. Martinon, K. Burns, J. Tschopp, *Mol.Cell* **2002**, *10*, 417–426.
[32] J. C. Reed, K. S. Doctor, A. Godzik, *Sci. STKE* **2004**, *239*, re9.
[33] S. Mariathasan, D. M. Monack, *Nat. Rev. Immunol.* **2007**, *7*, 31–40.
[34] A. Natarajan, R. Ghose, J. M. Hill, *J. Biol. Chem.* **2006**, *281*, 31863–31875.
[35] K. Saito, M. Inoue, S. Koshiba, T. Kigawa, S. Yokoyama, RIKEN Structural Genomics/Proteomics Initiative (RSGI), unpublished results.
[36] F. Espejo, M. E. Patarroyo, *Biochem. Biophys. Res. Commun.* **2006**, *340*, 860–864.
[37] T. A. Soares, X. Daura, C. Oostenbrink, L. J. Smith, W. F. van Gunsteren, *J. Biomol. NMR* **2004**, *30*, 407–422.
[38] R. D. Lins, P. H. Hünenberger, *J. Comput. Chem.* **2005**, *26*, 1400–1412.
[39] C. Oostenbrink, A. Villa, A. E. Mark, W. F. van Gunsteren, *J. Comput. Chem.* **2004**, *25*, 1656–1676.
[40] C. Oostenbrink, T. A. Soares, N. F. A. van der Vegt, W. F. van Gunsteren, *Eur. Biophys. J.* **2005**, *34*, 273–284.
[41] D. P. Geerke, W. F. van Gunsteren, *ChemPhysChem* **2006**, *7*, 671–678.
[42] H. R. Bosshard, D. N. Marti, I. Jelesarov, *J. Mol. Recognit.* **2004**, *17*, 1–16.
[43] R. J. Zauhar, R. S. Morgan, *J. Mol. Biol.* **1985**, *186*, 815–820.
[44] C. Lim, D. Bashford, M. Karplus, *J. Phys. Chem.* **1991**, *95*, 5610–5620.
[45] D. Sitkoff, K. A. Sharp, B. Honig, *J. Phys. Chem.* **1994**, *98*, 1978–1988.
[46] D. J. States, M. Karplus, *J. Mol. Biol.* **1987**, *197*, 122–130.
[47] J. Antosiewicz, J. A. McCammon, M. K. Gilson, *J. Mol. Biol.* **1994**, *238*, 415–436.
[48] E. Demchuk, R. C. Wade, *J. Phys. Chem.* **1996**, *100*, 17373–17387.
[49] M. Schaefer, M. Sommer, M. Karplus, *J. Phys. Chem. B* **1997**, *101*, 1663–1683.
[50] A. Yang, M. R. Gunner, R. Sampogna, K. Sharp, B. Honig, *Proteins* **1993**, *15*, 252–265.
[51] C. J. Gibas, S. Subramaniam, *Biophys. J.* **1996**, *71*, 138–147.
[52] H. W. T. van Vlijmen, M. Schaefer, M. Karplus, *Proteins* **1998**, *33*, 145–158.
[53] S. T. Russell, A. Warshel, *J. Mol. Biol.* **1985**, *185*, 389–404.
[54] Y. Y. Sham, Z. T. Chu, A. Warshel, *J. Phys. Chem. B* **1997**, *101*, 4458–4472.
[55] G. S. Del Buono, F. E. Figueirido, R. M. Levy, *Proteins* **1994**, *20*, 85–97.
[56] C. N. Schutz, A. Warshel, *Proteins Struct. Funct. Genet.* **2001**, *44*, 400–417.
[57] W. F. van Gunsteren, S. R. Billeter, A. A. Eising, P. H. Hünenberger, P. Krüger, A. E. Mark, W. R. P. Scott, I. G. Tironi, *Biomolecular Simulation: The GROMOS96 Manual and User Guide*, Verlag der Fachvereine, Zürich, **1996**.
[58] W. R. P. Scott, P. H. Hünenberger, I. G. Tironi, A. E. Mark, S. R. Billeter, J. Fennen, A. E. Torda, T. Huber, P. Krüger, W. F. van Gunsteren, *J. Phys. Chem. A* **1999**, *103*, 3596–3607.
[59] H. J. C. Berendsen, J. P. M. Postma, W. F. van Gunsteren, J. Hermans, *Interaction Models for Water in Relation to Protein Hydration: Intramolecular forces*, Reidel, Dordrecht, **1981**, 331–342.
[60] X. Daura, A. E. Mark, W. F. van Gunsteren, *J. Comput. Chem.* **1998**, *19*, 535–547.
[61] L. J. Smith, C. M. Dobson, W. F. van Gunsteren, *Proteins* **1999**, *36*, 77–86.
[62] J.-P. Ryckaert, G. Ciccotti, H. J. C. Berendsen, *J. Comput. Phys.* **1977**, *23*, 327–341.
[63] J. A. Barker, R. O. Watts, *Mol. Phys.* **1973**, *26*, 789–792.
[64] I. G. Tironi, R. Sperb, P. E. Smith, W. F. van Gunsteren, *J. Chem. Phys.* **1995**, *102*, 5451–5459.
[65] T. N. Heinz, W. F. van Gunsteren, P. H. Hünenberger, *J. Chem. Phys.* **2001**, *115*, 1125–1136.

 © 2008 Wiley-VCH Verlag GmbH & Co. KGaA, Weinheim

[66] H. J. C. Berendsen, J. P. M. Postma, W. F. van Gunsteren, A. DiNola, J. R. Haak, *J. Chem. Phys.* **1984**, *81*, 3684–3690.
[67] M. Christen, P. H. Hünenberger, D. Bakowies, R. Baron, R. Bürgi, D. P. Geerke, T. N. Heinz, M. A. Kastenholz, V. Kräutler, C. Oostenbrink, C. Peter, D. Trzesniak, W. F. van Gunsteren, *J. Comput. Chem.* **2005**, *26*, 1719–1751.
[68] W. Kabsch, C. Sander, *Biopolymers* **1983**, *22*, 2577–2637.

Received: July 31, 2007
Published online on March 17, 2008

 © 2008 Wiley-VCH Verlag GmbH & Co. KGaA, Weinheim